©*Proc. Indian natn. Sci. Acad.*, 47, A, Supplement No. 2, 1981, pp. 49–63

Printed in India

Near Space (Magnetospheric Electric Fields)

LARGE SCALE AND SMALL SCALE ELECTRIC FIELD DISTRIBUTION IN THE MAGNETOSPHERE

J. LEMAIRE

Institute for Space Aeronomy, 3, Av. Circulaire, B. 1180 Brussels, Belgium

(Communicated by A. P. Mitra, F.N.A.)

(*Received 22 April 1981*)

The electric field in the magnetosphere is patchy and irregular because of the presence of plasma irregularities.

1. There are charge separation electric fields of the order of several mV/m at the edges of plasma clouds. These microscopic electrostatic fields are perpendicular to the interface between regions filled with plasmas of different densities, temperatures or compositions. They are confined in thin double layers and have in general components parallel and perpendicular to the local magnetic field.
2. Secondly, there are convection electric fields arising from the bulk velocity of plasma irregularities with respect to the average background plasma. Impulsive penetration of magnetosheath plasma filaments is a source for these plasma irregularities and for their relative motions in the Plasma Boundary Layer. The distribution of these small scale convection electric fields is as patchy as the plasma distribution itself; their intensity is of the order of 1mV/m.
3. The third category of electric field is the large scale convection electric field (associated with corotation and overall motion of the magnetospheric plasma). Its intensity is of the order of 0.5 mVm (or less) in the vicinity of the magnetopause. High latitude pressure gradients in the atmosphere and momentum transferred impulsively from intruding solar wind plasma irregularities to the ionosphere determine the two-cells circulation in the polar ionosphere, and, consequently, influence the large scale flow pattern in the outer magnetosphere. The simple dawn-dusk electric field model, and the more detailed E3H electric field model, are two examples which can be tested with ATS 5 & 6 or other *in situ* space-craft observations.
4. Finally there are induced electric fields which are produced by time variations of the local magnetic field intensity. The daily wobble of the decentered and tilted magnetic dipole is a cause of induced *E*-field in the magnetosphere. Solar wind kinetic pressure variations at the magnetopause is another source of induced *E*-fields. The formation and decay of a Ring Current in the magnetosphere causes also time varying magnetic fields in the outer magnetosphere.

Keywords: Electric Field-Distribution; Magnetosphere; Plasma Irregularities; Ring Current.

Electrostatic Fields

The first magnetospheric electric field was deduced by Axford and Hines (1961) from high latitude phenomena and geomagnetic storm observations. Figure 1 shows the equatorial cross-section of constant potential surfaces ($\phi = ct$) for this electric field distribution. The electric field intensity is given by

$$E = -\text{ grad } \phi \qquad \ldots(1)$$

It can be seen that the largest electric field intensities are concentrated in the post-midnight sector where the spacing between constant ϕ curves is the smallest. Furthermore, according to this first theoretical model, the last closed equipotential extends up to the magnetopause, It became evident after 1961 that the plasma is corotating in the inner magnetosphere (inside the circle $L = 4$ of Fig. 1). The prevailing electric field at $L < 4$–5 is equal to the classical corotation electric field as described by Hones and Bergeson (1965). Whistler observations as well as incoherent radar measurements at low and mid-latitudes have been used to determine the equipotential curves in that inner region of the magnetosphere. Fig. 2 shows the constant lines for $L = 5$ as deduced by Richmond (1976).

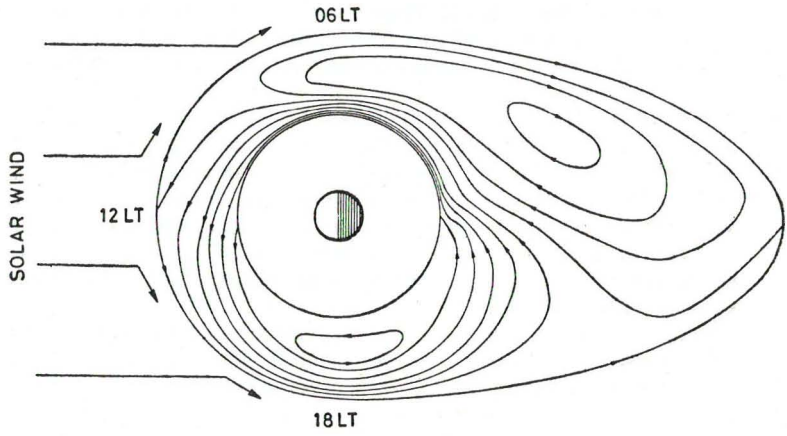

Fig. 1. Equatorial cross section of the magnetosphere. The solid lines correspond to equipotential contours of the Axford and Hines (1961) electric field model deduced from high latitude and geomagnetic-storm observations. Note the large electric field intensity in the post-midnight local time sector.

Using whistler observations, Carpenter discovered in 1963 a characteristic knee in the equatorial density distribution (see lower panel of Fig. 3). This sharp discontinuity in the cold plasma profile was called the plasmapause. The plasmapause is a field aligned boundary which resembles a doughnut encircling the earth. The local time dependence of the equatorial section has been determined by Carpenter (1966) from whistler measurements. It is shown by dotted lines in Fig. 4. It can be seen that it has a characteristic dawn-dusk asymmetry indicated by a bulge in the dusk local time sector.

To account for this bulge and for the tear drop of the plasmapause, *ad hoc* magnetospheric electric fields were introduced in 1967 by Brice and by Nishida

(1966). The last closed equipotential of their E-field models simulates the local time dependence of the actual plasmapause. A simpler version of this new type of electric field is the uniform dawn-dusk E-field whose constant ϕ curves are shown in Fig. 4 by dashed lines.

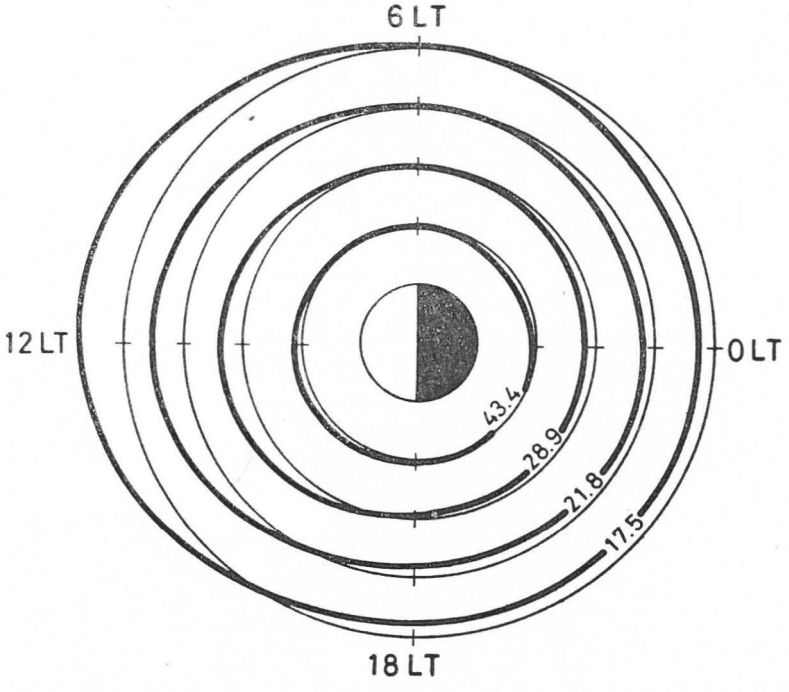

FIG. 2. Equatorial cross section of the inner magnetosphere. The solid lines correspond to equipotential contours deduced by Richmond (1976) from ionospheric plasma drift velocities obtained at low latitude incoherent scatter and whistler observing stations. Note that the closed equipotential contours do not differ much from those of the corotation electric field, for $L < 5$.

The position of the stagnation point in this analytical E-field model is a mathematical singularity which determines the position of the last closed equipotential and, presumably, the plasmapause according to the theory of Brice (1967), Nishida (1966) and Kavanagh *et al.* (1968). Indeed plasma convecting with the electric drift velocity

$$\mathbf{V}_E = \mathbf{E} \times \mathbf{B}/B^2 \qquad \ldots(2)$$

is corotating and trapped on closed streamlines parallel to the constant ϕ lines. However, plasma convecting parallel to open equipotentials eventually crosses the magnetopause at the frontside and escapes as described by Nishida (1966). A diffusive equilibrium density distribution can, therefore, build up inside the last closed equipotential surface, but not outside. Hence, the plasmapause knee could result in such an E-field provided there is somewhere a stagnation point where $\mathbf{E}$ and $\mathbf{V}_E$ are equal to zero.

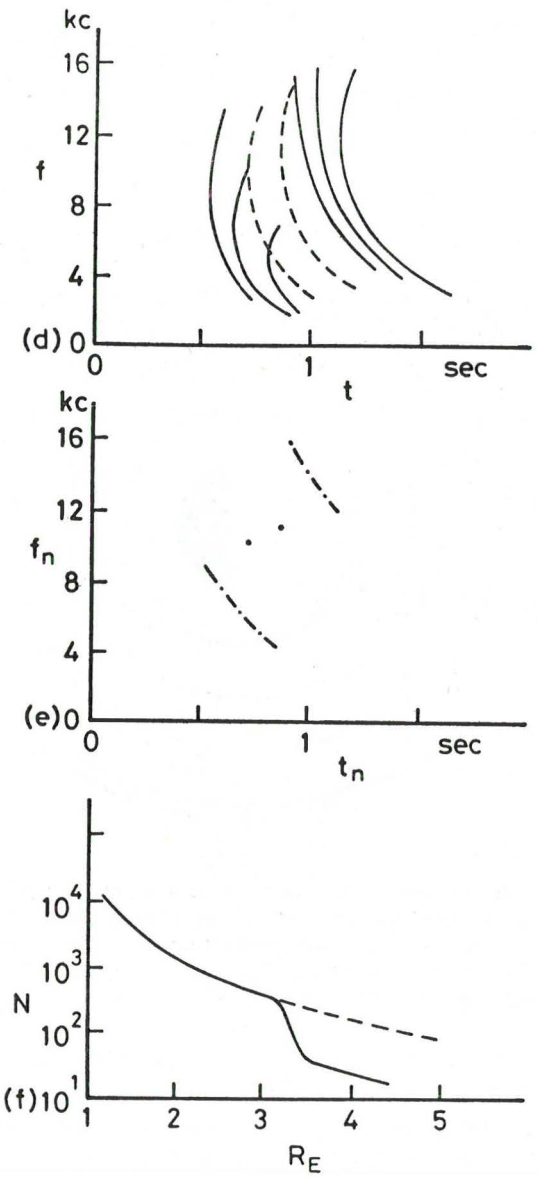

FIG. 3. The upper panel shows observed whistler frequencies *vs.* time. The nose frequencies (f_n) *vs.* propagation times (t_n) are plotted in the central panel. The lower panel shows the equatorial plasma density (N) [: deduced from the propagation time (t_n)], *vs.* the equatorial distance (L) [: deduced from the corresponding whistler nose frequency (f_n)] [after Carpenter . (1963)].

In 1972, Mc Ilwain deduced an empirical magnetospheric electric field which fits his observations of electrons and ions made on board the ATS5 spacecraft at geostationary orbit: i. e., for $L = 6.7$. Two years later, Mc Ilwain (1974) confirmed and refined his electric field model which is shown in Fig. 5.

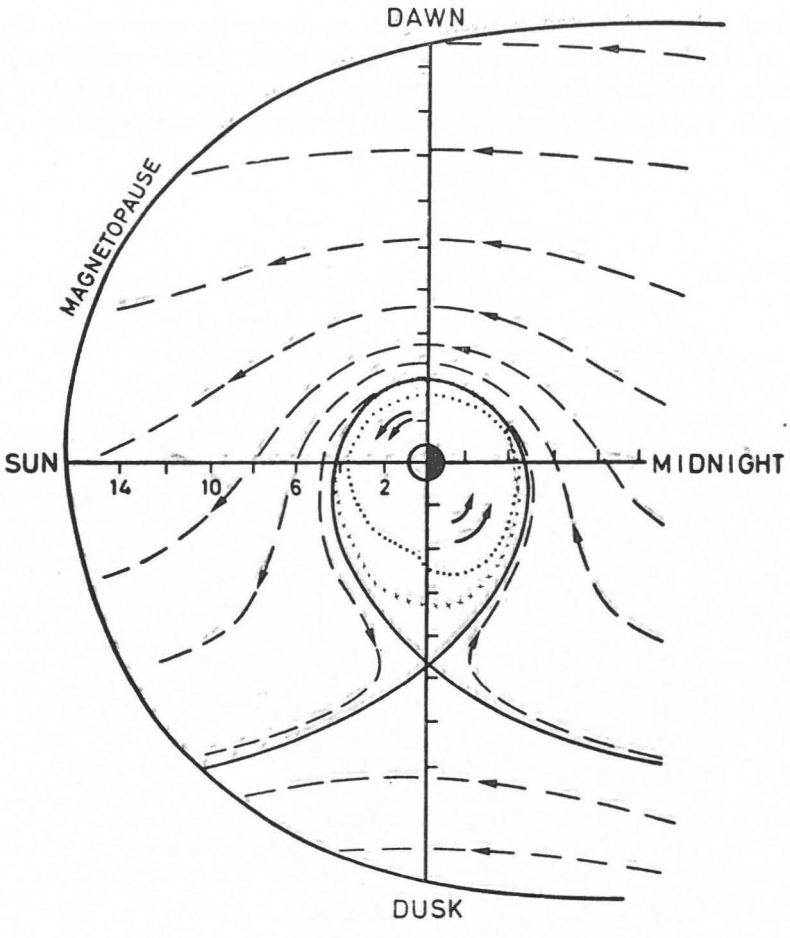

FIG. 4. Equatorial cross section of the magnetosphere. The dashed lines are equipotential contours of the uniform dawn-dusk electric field introduced by Kavanagh *et al.* (1968). The solid line is the last closed equipotential contour. The equatorial location of the plasmapause deduced from Whistler observations by Carpenter (1966) is indicated by dots. The average plasmapause position deduced from OGO 5 observations by Chappell *et al.* (1971) is given by crosses.

It is interesting to note that this empirical field model resembles more closely to the early model of Axford and Hines (Fig. 1) than the uniform dawn-dusk model (Fig. 4). Indeed the E3H model has also a large intensity in the post-midnight sector which implies super rotation for $L > 4$ between 0000 LT and 0600 LT. Recent incoherent radar observations support well this prediction.

Furthermore, as in the model of Axford and Hines, the last closed equipotential surface extends up to the magnetopause, or at least up to the Plasma Boundary Layer.

Fig. 6 shows ATS6 spectrograms obtained at geostationary orbit for steady geomagnetic conditions ($K_p = 1-2$). Fig. 7 has been drawn with the same scale as Fig. 6. The solid line in Fig. 7 shows the calculated Universal Times for which

ATS6 should have detected particles of a given energy, assumed to have been injected at the inner edge of the Plasma Boundary Layer and to have drifted subsequently in the E3H electric field shown in Fig. 5. It is remarkable how well the traces in Fig. 7 fit the actual edge of the bright area in the spectrograms of Fig. 6.

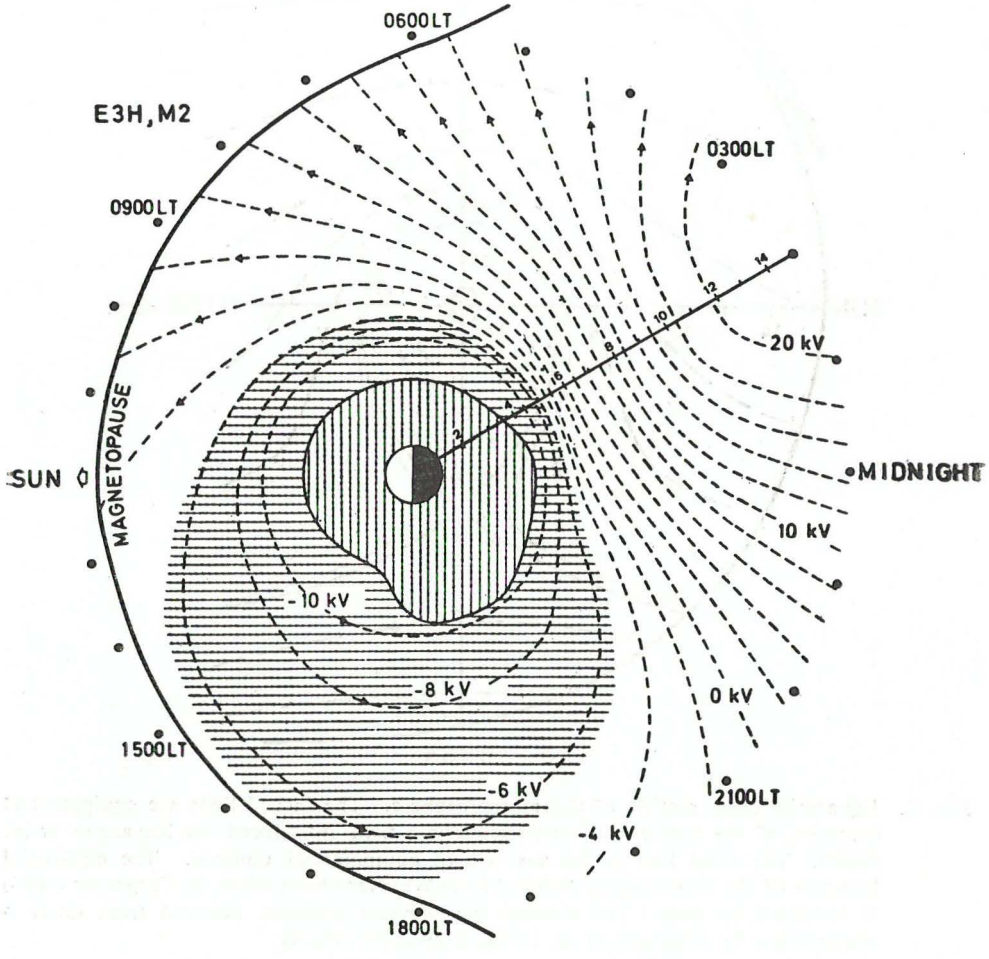

FIG. 5. Equatorial section of the magnetosphere. The dashed lines are equipotential contours of Mc Ilwain E3H electric field model deduced from ATS5 spectrograms during quiet geomagnetic conditions (K_p=1–2). The shaded area is the cross section of the region containing closed $\mathbf{E}\times\mathbf{B}/B^2$ convection streamlines. Note that the convection electric field intensity has a maximum in the post-midnight sector as in the Axford and Hines (1961) model.

The dotted line in the lower panel corresponds to the Universal Times (or Local Times) for which energetic protons emitted at the Plasma Boundary Layer or in the magnetotail reach ATS6 orbit after having passed through the denser regions in the magnetosphere at smallest L-values. Particles on such orbits are likely to have been scattered and will be absent in the observed spectrogram. It

is interesting to see that the dark oblique strip seen in the lower part of Fig. 6 follows rather accurately the dotted line in Fig. 7 corresponding to the particles with the deepest penetration in the magnetosphere. This leads us to the conclusion that, at least for a geomagnetically quiet day, the E3H field model approximates satisfactorily the actual magnetospheric electric field distribution (Lemaire & Mc Ilwain, 1980).

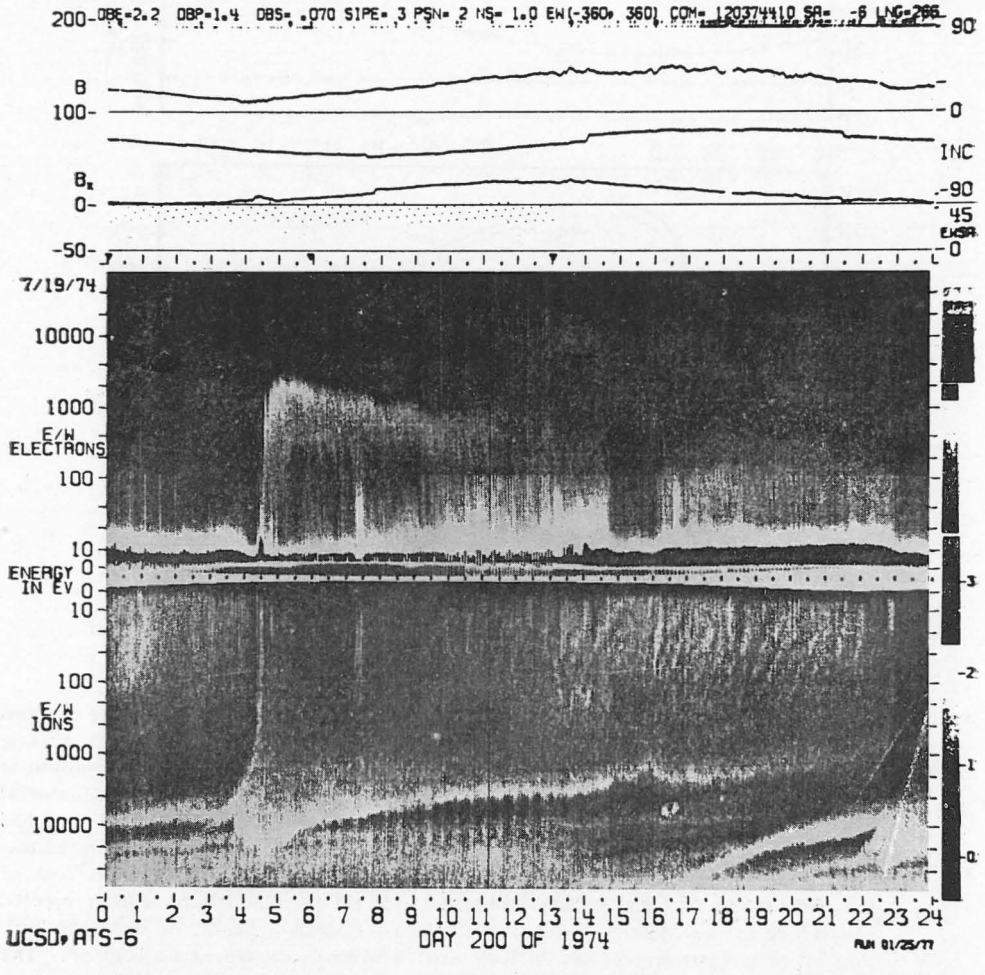

FIG. 6. Electron and ion spectrograms obtained with the UCSD detectors on board ATS6, as a function of Universal Time, for the day 19 July 1974. Fluxes of electrons and ions for a given energy and at a given Universal Time (or local time: LT=UT—6.33) are highest in the brightest areas. The magnetic field intensity (B) along the ATS6 geostationary orbit is shown in the upper panel.

Electric field models like those of Figs. 1 or 5 allow for the source of newly injected particles detected at geostationary orbit to be located somewhere along the dusk flank of the magnetopause or of the Plasma Boundary Layer. On the

contrary, an electric field of the type shown in Fig. 4 does not allow magnetosheath particles to drift directly in the inner magnetosphere from the frontside or duskside of the magnetopause. For a uniform dawn-dusk *E*-field model, substorm injected particles necessarily have their source somewhere down the magnetotail.

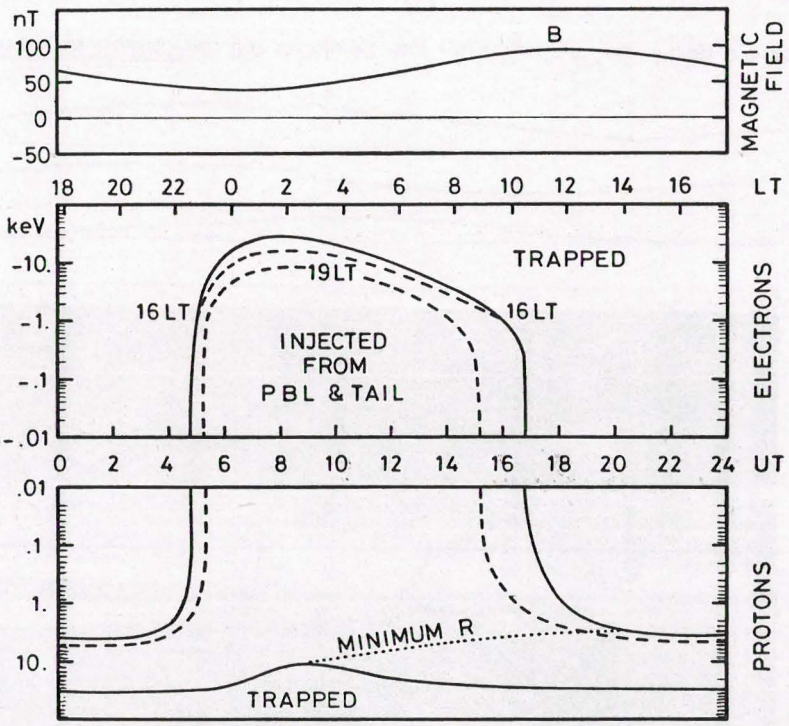

FIG. 7. Characteristic boundaries in ATS6 energy spectrograms. Solid curves separate energies of trapped particles from those of particles injected into the magnetotail or drifting in from the Plasma Boundary Layer. Mc Ilwain's E3H electric field distribution is assumed in the calculation of the drift paths of electrons and ions in the equatorial plane of the magnetosphere. For example, an electron of 1 KeV, detected along ATS6 geostationary orbit at 0400 UT (or 2140 LT), was drifting eastwardly on a closed trajectory, i.e., a drift path not intersecting the magnetopause; however, the electrons of the same energy (+1 KeV) observed beyond 0450 UT (or 2230 LT) have been injected somewhere at the Magnetopause, at the Plasma Boundary Layer, or down the Tail. Protons of energies larger than 30 KeV drift westwards on closed trajectories. The dotted lines (16 LT and 19 LT) give the UT's (or LT's) for which particle of a given energy and injected at 16 LT and 19 LT along the magnetopause, are actually detected at the ATS6 geostationary orbit. The dotted curve gives the energies of particles with the deepest penetration in the magnetosphere. Particles of these energies are most likely to be scattered and missing in the ATS6 spectrograms.

Of course, all these static electric field models would be expected to match all ATS5 and 6 observations, especially for geomagnetically disturbed days. Under disturbed conditions, ATS5 and 6 spectrograms are very much irregular and are hardly interpretable in terms of any electrostatic field distribution.

Time-Dependent Electric Fields

When the magnetic field intensity at ground and in the magnetosphere changes because of some variation in the solar wind flow, induced electric field are produced in the magnetosphere. These time-dependent electric fields satisfy Maxwell's equation

$$\frac{\partial \mathbf{B}}{\partial t} = -\,\mathbf{curl}\ \mathbf{E} \qquad \ldots(3)$$

The importance of such *E*-fields has been emphasised by Heikkila and Pellinen

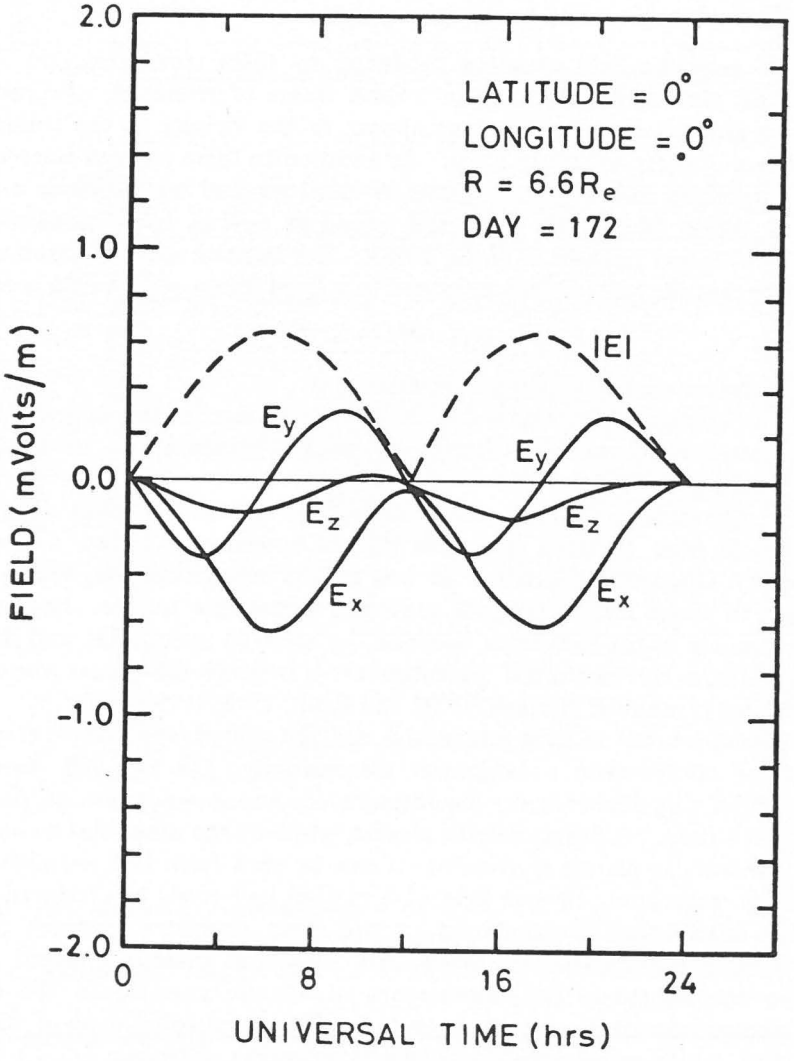

Fig. 8. Induced electric field intensities at geostationary orbit produced by the diurnal rotation of the tilted magnetic dipole. The component of the induced electric field vectors have been evaluated at geostationary orbit for a point at zero longitude. [after Mroz *et al.*, (1979)].

Fig. 10 shows for example the electric potential distribution required in a collisionless model to maintain quasi-neutrality (and satisfy Poisson's equation) everywhere along a cleft magnetic flux tube filled from below with cold ionospheric O^+ & H^+ ions and electrons; warm magnetosheath like electrons and protons are injected from the top. The maximum parallel electric field generated in the double layer at 22,000 km altitude is 100 mV/m. Parallel electric fields of this nature and of this intensity have probably been observed recently in the magnetosphere (*see* Mozer, 1980).

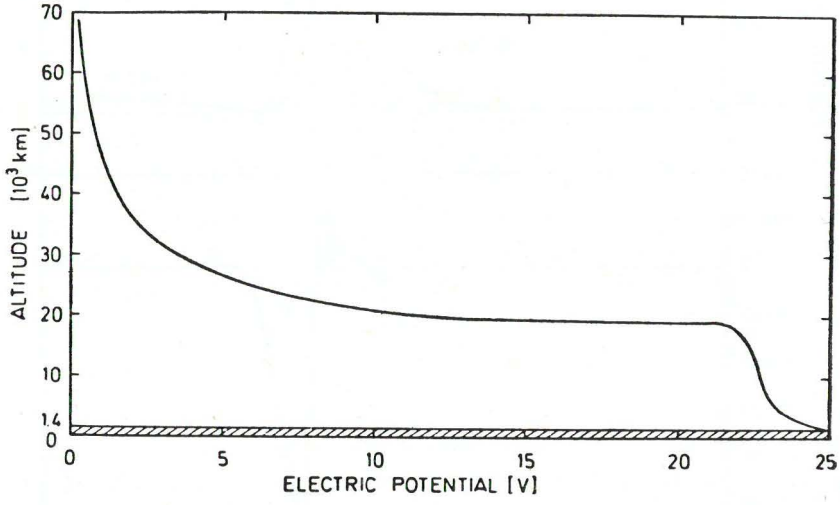

FIG. 10. Electric potential distribution along a dipole magnetic flux tube filled from below with cold ionospheric plasma and from above with warm magnetosheath like plasma. The field aligned electric potential has a sharp gradient between 20000 and 30000 km. The resulting large parallel electric field is necessary to maintain quasi-neutrality in the cold and warm interacting plasmas [after Lemaire & Scherer, (1978)].

Fig. 11 illustrates another physical mechanism which produces patchy and time-dependent electric fields in the magnetosphere. Indeed, let us consider a plasma density irregularity in the equatorial region of the magnetosphere, and assume that the electric field far outside this plasma element is zero (or that we are in a frame of reference moving with the convection velocity of the external plasma). The electrons and ions trapped inside this field aligned volume element will drift in opposite direction under the action of the gravitational force $m_{i(e)}\mathbf{g}$., and will give rise to polarization charges at the eastern and western edges of the plasma irregularity. A charge separation electric field builds up in the vicinity of this plasma element, and produces an $\mathbf{E} \times \mathbf{B}/B^2$ drift in the direction of the total applied force $V \triangle nmg$ applied to the excess of mass $V \triangle nm$ stored in the plasma density irregularity (Longmire, 1963). If the magnetic field lines passing through this plasma element would be rooted in a perfectly insulating atmosphere, the plasma irregularity would be accelerated indefinitely in the direction of the total force. Consequently, if, ideally, the integrated Pedersen conductivity (Σ_p) were

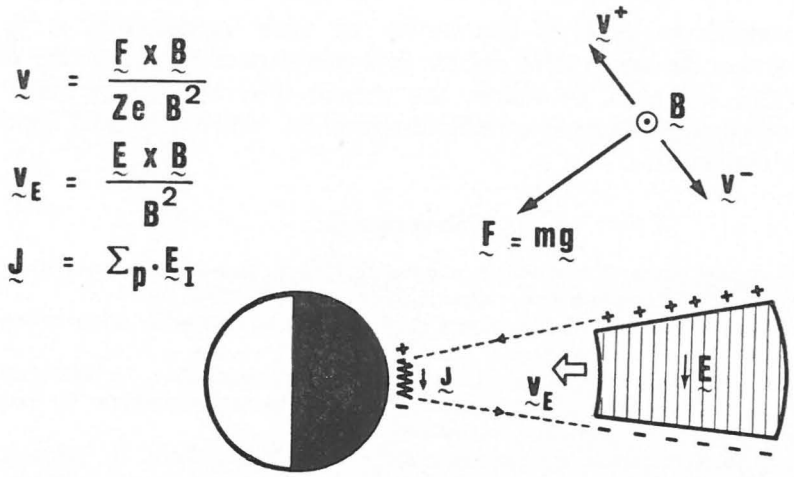

FIG. 11. Illustration of the charge separation electric field produced in the vicinity of a cold plasma density element by oppositely directed gravitational drifts of electrons and ions (after Lemaire, 1975). The maximum electrostatic potential difference that can build up between the east and west sides of the plasma element is determined by the value of the integrated Pedersen conductivity (Σ_p) in the ionospheric *E*-region. The resulting plasma interchange velocity (V_{IC}) is directed parallel to the external force ($\triangle_{nm}$ g) and its maximum value is inversely proportional to Σ_p.

equal to zero, the electric field intensity inside the plasma volume keeps increasing and its bulk speed would grow at the rate:

$$\frac{dv}{dt} = g \qquad \ldots(6)$$

However, the ionosphere is not an ideal insulator and Pedersen currents leak through the *E*-region and discharge the potential difference between the two sides of the plasma element. Therefore, a constant fall velocity is eventually reached for which the loss rate of potential energy is equal to the rate of Joule dissipation in the ionosphere ($\Sigma_p E_I^2$). It can be shown that this maximum plasma interchange velocity (V_{IC}) is proportional to the excess of mass ($V \triangle nm$) and inversely proportional to Σ_p.

Therefore V_{IC} is zero when $\triangle n = 0$ or when $\Sigma_p = \infty$ (i. e., for a superconducting ionosphere).

From this example, it can be concluded that external forces (gravitational, centrifugal or inertial) can produce irregular and time dependent electric fields in the magnetosphere. But curvature drift and gradient-*B* drifts can also generate similar charge separation *E*-field inhomogeneities. Conversely, any wind motion or electric field in the ionosphere can map up in the magnetosphere. This can be another major source of patchy and fluctuating *E*-field in the Earth's magnetosphere.

CONCLUSION

In conclusion, it can be said that there are plenty of mechanisms which can contribute to make the magnetospheric *E*-field much less uniform than has often

been assumed. In view of the variety of such mechanisms, it is even surprising that the static E3H electric field model does in fact fit the observations of Fig. 6 so well. Of course, the present observations were made during steady and quiet geomagnetic conditions typical for which the E3H model was originally designed for.

References

Axford, W. I., and Hines, C. O. (1961) A unifying theory of high-latitude geophysical phenomena and geomagnetic storms. *Can. J. Phys.*, **39**, 1433–1464.

Block, L. P. (1977) Potential double layers in the ionosphere. *Cosmic Electrodynamics*, **3**, 349–376.

Brice, N. M. (1967) Bulk motion of the magnetosphere. *J. geophys. Res.*, **72**, 5193–5211.

Carpenter, D. L. (1963) Whistler evidence of the knee in the magnetospheric ionization density profile. *J. geophys. Res.*, **68**, 1675–1682.

———(1966) Whistler studies of the plasmapause in the magnetosphere. I. Temporal variations in the position of the knee and some evidence of plasma motions near the knee. *J. geophys. Res.*, **71**, 693–709.

Chappell, C. R., Harris, K. K. and Sharp, G. W. (1971) The dayside of the plasmasphere. *J. geophys. Res.*, **76**, 7632–7647.

Evans, D. S. (1974) Precipitating electron fluxes formed by a magnetic field aligned potential difference. *J. geophys. Res.*, **79**, 2853–2858.

Fälthammar, C. G. (1977) Generation mechanisms for magnetic field-aligned electric fields in the magnetosphere. TRITA-EPP-77-21, presented at the Third General Scientific Assembly of IAGA, Seattle, Wash., 1977.

Heikkila, W. J., and Pellinen, R. J. (1977) Localized induced electric field within the magnetotail. *J. geophys. Res.*, **82**, 1610–1614.

Hones, E. W. Jr., and Bergeson, J. E. (1965) Electric field generated by a rotating magnetized sphere. *J. geophys. Res.*, **70**, 4951–4958.

Kavanagh, L. D. Jr., Freeman, J. W. Jr., and Chen, A. J. (1968) Plasma flow in the magnetosphere. *J. geophys. Res.*, **73**, 5511–5519.

Lemaire, J. (1975) The mechanisms of formation of the plasmapause. *Ann. Geophys.*, **31**, fasc. 1, 175–190.

———(1977) Impulsive penetration of filamentary plasma elements into the magnetospheres of the Earth and Jupiter. *Planet. Space. Sci.*, **25**, 887–890.

Lemaire, J., and Burlaga, L. F. (1976) Diamagnetic boundary layers: a kinetic theory. *Astrophys. Space. Sci.*, **45**, 303–325.

Lemaire, J., and McIlwain, C. E. (1980) *(unpublished material)*

Lemaire, J., and Roth, M. (1978) Penetration of solar wind plasma elements into the magnetosphere. *J. atmos. terr. Phys.*, **40**, 331–335.

Lemaire, J., and Scherer, M. (1978) Field aligned distribution of plasma mantle and ionospheric plasmas. *J. atmos. terr. Phys.*, **40**, 337–372.

Longmire, C. L. (1963) *Elementary Plasma Physics.* Interscience, New York.

McIlwain, C. E. (1972) Plasma convection in the vicinity of the geosynchronous orbit, In: "*Earth Magnetospheric Processes*," 268–279 (*Ed.* B. M. McCormac). D. Reidel Publ. Co., Dordrecht-Holland, 1972.

———(1974) Substorm injection boundaries in "*Magnetospheric Physics*," 143–154 (*Ed.* B. M. McCormac). D. Reidel Publ. Co., Dordrecht-Holland, 1974.

Mozer, F. (1980) Parallel electric field measurements. Paper presented at Chapman Conference on "*High Latitude Electric Fields in the Magnetosphere and Ionosphere*," Yosemite, California, January 30–February 2, 1980.

Mroz, G. J., Olson, W. P., and Pfitzer, K. A. (1979) Induced magnetospheric electric fields, In: "*Quantitative Modelling of Magnetospheric Processes*," *Geophys. Monograph Sci.*, **21**, (*Ed.:* W. P. Olson). AGU, Washington D. C., 1979.

Nishida, A. (1966) Formation of plasmapause, or magnetospheric plasma knee, by the combined action of magnetospheric convection and plasma escape from the tail. *J. geophys. Res.*, **71**, 5669–5679.

Richmond, A. E. (1976) Electric field in the ionosphere and plasmasphere on quiet days. *J. geophys. Res.*, **81**, 1447–1450.

Roth, M. (1978) Structure of tangential discontinuities at the magnetopause : the nose of the magnetospause. *J. atmos. terr. Phys.*, **40**, 323.

———(1979) A microscopic description of interpenetrated plasma regions. *Proc. Magnetospheric Boundary Layers Cont. Alpbach*, 11–15 June 1979, ESA SP-148, August 1979, p. 295.

———(1980) La structure interne de la magnetopause. *Ph.D. Thesis*, Brussels Univ., 1980, *Aeronomica Acta* A *n°* **221**.